RSC Advances

PAPER

View Article Online
View Journal | View Issue

Cite this: *RSC Adv.*, 2014, **4**, 43142

Impact of dithienyl or thienothiophene units on the optoelectronic and photovoltaic properties of benzo[1,2,5]thiadiazole based donor–acceptor copolymers for organic solar cell devices†

Andrew J. Pearson,‡[a] Darren C. Watters,§[a] Hunan Yi,[b] Mohd S. Sarjadi,[b] Luke X. Reynolds,[c] Pier P. Marchisio,[d] James Kingsley,[d] Saif A. Haque,[c] Ahmed Iraqi*[b] and David G. Lidzey*[a]

Received 16th July 2014
Accepted 21st August 2014

DOI: 10.1039/c4ra07186g

www.rsc.org/advances

We report a comparative study on four donor–acceptor benzothiadiazole-based copolymers containing dithienyl or thienothiophene moieties for application in organic photovoltaic (OPV) devices. Bulk-heterojunction OPV devices are fabricated having power conversion efficiencies ranging between 4 and 6%. Morphological, spectroscopic and charge-transport measurements are used to investigate the influence of either the dithienyl or thienothiophene moieties on the structure and photophysical properties of the copolymer and copolymer:$PC_{71}BM$ blend films and rationalise the solar cell characteristics. Although all copolymer:$PC_{71}BM$ blends exhibit comparable hole polaron yields, solar cell devices with the highest power conversion efficiencies are correlated with increased charge-carrier mobility of the copolymer and enhanced aggregation of $PC_{71}BM$ in the blend.

Introduction

Solution-processable photovoltaic devices are a promising technology for low-cost solar energy conversion, with organic photovoltaic devices (OPVs) attracting significant attention from a wide range of traditional research fields over the past decade.[1–4] OPV devices that employ blends of conjugated polymers and fullerene derivatives in the photoactive layer in a bulk-heterojunction (BHJ) architecture have demonstrated a steady rise in efficiency and lifetime in recent years.[1,5] This rise has, in part, been due to the large number of novel electron donating semiconductors that have been synthesised. In particular, donor–acceptor copolymers with alternating electron-rich and electron-deficient heterocycles along the conjugated backbone have proven to be promising semiconductor materials that have low optical band-gaps, and can thus efficiently harvest a relatively large portion of the visible and near-IR regions of the solar spectrum.[6–8] Benzothiadiazole (BT) is one example of an electron-deficient moiety that can be included in a donor–acceptor copolymer. Many examples exist where this unit is flanked by thiophene moieties and combined with a suitable electron donor such as 2,7-carbazole,[9] fluorene,[10] cyclopentadithiophene[11] and benzodithiophene.[12,13] When blended with fullerene derivatives such as PCBM or $PC_{71}BM$ in an OPV device, power conversion efficiencies of up to 8% have been achieved under optimised processing conditions.[13]

One strategy to further improve the light-harvesting efficiency of BT containing copolymers is to reduce their optical band-gaps by altering adjacent units with other heterocycles such as selenophene.[14–17] Fused heterocycles may also be used to modify the optical bandgap of the copolymer; an approach that forms the basis of this work. The synthesis of PFDT2BT-8 and PCDT2BT-8 have been reported previously,[18,19] with devices incorporating PFDT2BT-8 exhibiting maximum PCEs above 6% after optimisation of the device architecture.[18] The copolymer PCDT2BT-8 is similar in structure to the relatively well-studied copolymer PCDTBT.[9,20–23] Here, addition of octyloxy groups to the BT unit has been shown to increase the solubility of PCDT2BT-8 in common processing solvents relative to PCDTBT. Furthermore, a reduction in the HOMO level of PCDT2BT-8 relative to PCDTBT has been shown to afford an increase in device open-circuit voltage.[19] Substitution of the two thiophene

[a]*Department of Physics & Astronomy, University of Sheffield, Hicks Building, Hounsfield Road, Sheffield, S3 7RH, UK. E-mail: d.g.lidzey@sheffield.ac.uk; Fax: +44 (0)114 222 3555; Tel: +44 (0)114 222 3501*

[b]*Department of Chemistry, University of Sheffield, Sheffield, S3 7HF, UK. E-mail: a.iraqi@sheffield.ac.uk; Fax: +44 (0)114 222 9303; Tel: +44 (0)114 222 9566*

[c]*Centre for Plastic Electronics and Department of Chemistry, Imperial College London, South Kensington Campus, Exhibition Road, SW7 2AZ, UK*

[d]*Ossila Ltd., Kroto Innovation Centre, Sheffield, S3 7RQ, UK*

† Electronic supplementary information (ESI) available: OPV device optimisation data, GIWAXS measurements of pure polymer films, AFM scans of blend film surface, PL spectra of neat and blend thin-films and OFET transfer and output characteristics. See DOI: 10.1039/c4ra07186g

‡ Present address: Cavendish Laboratory, JJ Thomson Avenue, Cambridge CB3 0HE, United Kingdom.

§ Present address: Ossila Ltd., Kroto Innovation Centre, Sheffield, S3 7RQ, UK.

units on PCDT2BT-8 and PFDT2BT-8 with thienothiophene moieties provides a further opportunity to modify the structural and optoelectronic properties of the copolymers. Synthesis of these structures affords two new polymers, namely PCDTTBT-8 and PFDTTBT-8. In this work a detailed physical study is undertaken to explore the optical and electronic properties of these four copolymers in order to understand their performance in OPV devices.

Results and discussion

The copolymers PCDT2BT-8 and PFDT2BT-8 were synthesised according to previous reports. Copolymers PCDTTBT-8 and PFDTTBT-8 were prepared using Suzuki coupling conditions upon reaction of 4,7-bis-(5-bromo-thieno[3,2-*b*]thiophen-2-yl)-5,6-bis-octyloxy-benzo[1,2,5]thiadiazole with 9-(heptadecan-9-yl)-2,7-bis(4,4,5,5-tetramethyl-1,3,2-dioxaborolan-2-yl)-9*H*-carbazole and 9,9-dioctylfluorene-2,7-diboronic acid bis(1,3-propanediol) ester respectively according to Scheme 1. The structures of all the copolymers studied are shown in Fig. 1, with detailed synthetic procedures provided in the Experimental methods.

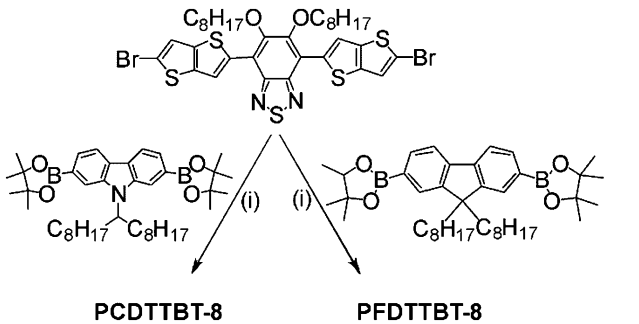

Scheme 1 (i) (a) $Pd(OAc)_2$/(*o*-tolyl)$_3$P (1/2), NEt_4OH, toluene/H_2O, 95 °C, 4 h. (b) PhBr, (c) $PhB(OH)_2$.

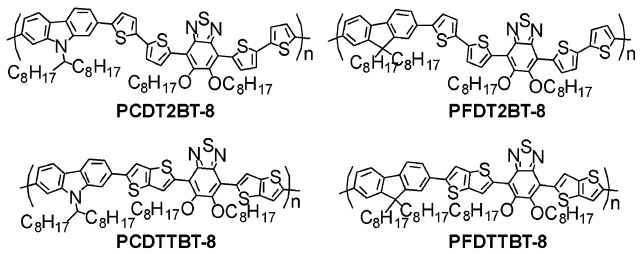

Fig. 1 Chemical structures of the copolymers used in this study.

All polymers were purified before use, and separated *via* Soxhlet extraction methods, with reaction yields above 80%. Gel permeation chromatography measurements from the polymerization reactions (using polystyrene standards) have shown weight average molecular weight values M_w ranging from 48 000 to 91 600 Da (Table 1) with polydispersity index values ranging from 1.47 to 2.98. All polymers displayed promising solubility in chlorinated solvents such as chloroform (CF), chlorobenzene (CB) and 1,2-dichlorobenzene (DCB).

Optical properties

Normalised UV-VIS absorption spectra of each copolymer in solution and thin-film are presented in Fig. 2. It can be seen that the structure of the absorption spectra for each copolymer are qualitatively similar, with the onset of absorption for thin-films being around 1.9 eV. These absorption spectra are in general characterised by two broad bands in the wavelength range 520–580 nm and 400–430 nm. At the wavelength of peak absorption, the molar extinction coefficients (ε) of all polymers exceed 58 000 L mol^{-1} cm^{-1}, with the most absorptive polymer being PCDTTBT-8 which has ε = 67 200 L mol^{-1} cm^{-1}.

We find a relative red-shift in optical absorption is observed for each copolymer when it is cast from solution into a thin-film. Such effects are likely attributed to an increased aggregation of polymer chains. Comparison of the absorption spectra from thienothiophene-based copolymers show that for the 2,7-carbazole derivatives, a relative red-shift in the onset of absorption is observed for PCDTTBT-8 compared to the polymer PCDT2BT-8. This difference is in qualitative agreement with several reports of band-gap reduction for thienothiophene containing copolymers relative to their thiophene counterparts.[24–26] However, no significant difference between the optical band-gap is observed for the fluorene-based copolymers PFDT2BT-8 and PFDTTBT-8. Note here that the absorption band located at approximately 420 nm for PFDT2BT-8 is apparently blue-shifted to 400 nm in the polymer PFDTTBT-8. It is possible that this change originates from variations in the degree of electronic delocalization along the conjugated backbone of each copolymer, or differences in molecular weight.

Electrochemical properties

Cyclic-voltammetry (CV) measurements were conducted on drop-cast polymer films in acetonitrile with tetrabutylammonium

Table 1 Physical characteristics of the copolymers used in this study

Polymer	M_n[a]/kDa	M_w[a]/kDa	PDI[a]	E^0_{ox}/V	E^0_{red}/V	HOMO[b]/eV	LUMO[b]/eV	Band gap[c]/eV	ε[d]/L mol^{-1} cm^{-1}
PCDT2BT-8	31.1	57.2	1.84	0.78	−1.72	−5.2	−3.3	1.95	58 500
PCDTTBT-8	18.6	48.0	2.58	0.79	−1.52	−5.3	−3.5	1.89	67 200
PFDT2BT-8	64.2	91.6	1.47	0.71	−1.45, −1.74	−5.3	−3.4	1.92	58 600
PFDTTBT-8	25.4	75.8	2.98	0.81	−1.70	−5.3	−3.2	1.94	58 400

[a] Determined by GPC against PS standards. [b] Determined by CV. [c] Estimated from the absorption onset in UV-VIS measurements of copolymer thin-films. [d] Measured at peak optical absorption.

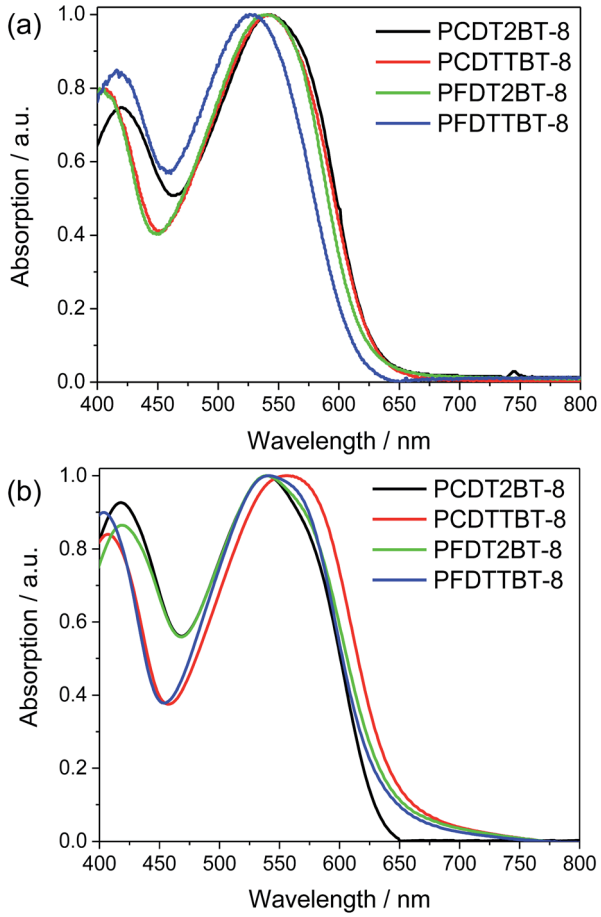

Fig. 2 Normalised UV-VIS absorption spectra of copolymers in (a) chloroform solvent and (b) deposited as thin-films from chloroform solvent.

perchlorate as an electrolyte (Fig. 3). The redox potentials of the different polymers are presented in Table 1 along with the values of the HOMO and LUMO levels for each copolymer in this study as determined from their onset of oxidation and reduction respectively. It can be seen that all copolymers have very similar HOMO levels which are located between −5.2 eV and −5.3 eV relative to vacuum, while relatively larger variations in the positions of their LUMO levels (located between −3.5 eV and −3.2 eV) were observed.

Photovoltaic, structural & charge transport properties

Solar cell devices in a standard architecture were fabricated to determine the photovoltaic efficiency of each copolymer when blended with the fullerene derivative $PC_{71}BM$. The device structure in each case was as follows: ITO/PEDOT:PSS (30 nm)/active layer (50–100 nm)/Ca (5 nm)/Al (100 nm). To optimise the morphology of the photoactive semiconductor blend layer for photovoltaic performance, we have explored the influence of the casting solvent, blend composition and the application of post-film deposition annealing treatments. In Fig. 4 and Table 2, the photovoltaic characteristics and efficiency parameters derived from the current–voltage measurements are presented for solar cell devices after active-layer optimisation. Device efficiency metrics for other solar cells prepared during the optimisation process, including the influence of active layer blend ratio, are presented in the ESI.†

As shown in Fig. 4, all optimised devices exhibit relatively efficient photovoltaic behaviour. We find that the optimum weight composition of each photoactive layer is 1 : 4 wt% copolymer:$PC_{71}BM$; a composition comparable to that used for other PCDTBT-derivatives.[14,18,19] The thickness of the photoactive semiconducting layer in each optimised device was found to be approximately 60 nm. Comparing the two carbazole containing copolymers PCDT2BT-8 and PCDTTBT-8, substitution of the thiophene heterocycles with thienothiophene permits the fabrication of photovoltaic devices having a PCE of 4%. For the best performing devices however, OPV devices utilising PCDT2BT-8 reach a maximum PCE of 4.1% whereas for OPV devices utilising PCDTTBT-8 a slightly higher PCE of 4.5% is determined. From Table 2 it is apparent that the improvement in PCE of the best PCDTTBT-8 devices relative to the PCDT2BT-8

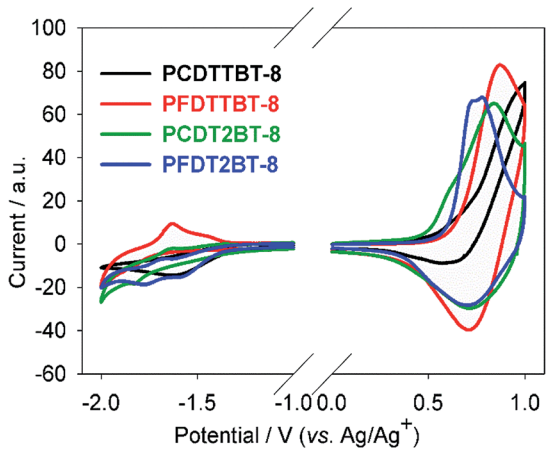

Fig. 3 Cyclic-voltammetry (CV) curves of polymer thin films on platinum disc electrodes (area 0.031 cm^2) at a scan rate of 100 mV s^{-1} in acetonitrile/tetrabutylammonium perchlorate (0.1 mol dm^{-3}).

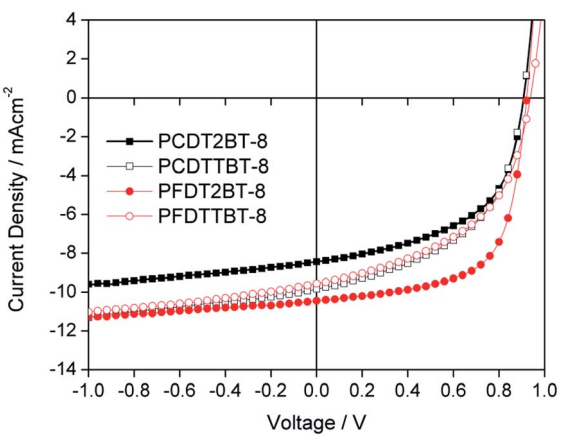

Fig. 4 Current–density *versus* voltage characteristics for copolymer:$PC_{71}BM$ OPV devices under 100 mW cm^{-2} AM1.5 illumination.

Table 2 Average solar cell metrics for optimized copolymer:$PC_{71}BM$ 1 : 4 wt% blend OPVs under 100 mW cm^{-2} AM1.5 illumination. PCE values in square brackets correspond to the maximum value determined from each sample set

Polymer	Solvent	Annealing	V_{OC}/V	J_{SC}/mA cm^{-2}	FF/%	PCE/%
PCDT2BT-8	CF	110 °C	0.88	−8.7	52	3.9 ± 0.2 [4.1]
PCDTTBT-8	CB	N/A	0.90	−9.6	47	4.1 ± 0.3 [4.5]
PFDT2BT-8	CF	N/A	0.91	−10.3	62	5.8 ± 0.2 [6.2]
PFDTTBT-8	CF	N/A	0.93	−9.5	46	4.1 ± 0.3 [4.4]

devices results from increased short-circuit current density (J_{SC}) (9.8 mA cm^{-2} and 8.7 mA cm^{-2} respectively).

This can be correlated with the relatively lower optical band-gap and higher molar extinction coefficient of PCDTTBT-8. Furthermore, comparison of the photovoltaic performance of PCDTTBT-8 (PCE of up to 4.5%) to a similar carbazole-based polymer described in the literature (PCTTBTC12) (PCE of 3.4%),[27] with dodecyloxy-substituents rather than octyloxy-substituents, also indicates a superior performance of PCDTTBT-8.

Comparing the photovoltaic efficiency of PFDT2BT-8:$PC_{71}BM$ blends with PFDTTBT-8:$PC_{71}BM$ blends, it can be seen that a relatively lower average PCE is obtained for the PFDTTBT-8 based OPV devices (4.1% against 5.8% for PFDT2BT-8:$PC_{71}BM$). This difference arises from a relatively lower FF and J_{SC} for the PFDTTBT-8 devices as the open-circuit voltage V_{OC} in each system is similar (0.93 compared with 0.91 V for PFDT2BT-8:$PC_{71}BM$). For OPV devices incorporating PFDT2BT-8 a maximum PCE of 6.2% is determined; the highest value in the material set studied.

A morphological study was undertaken to characterise the nanostructure of the blend films. Specifically, grazing-incidence wide-angle X-ray scattering (GIWAXS) was employed to characterise the degree of nanoscale crystallinity in the blend films. These measurements were complimented by atomic force microscopy (AFM) imaging of the sample surface for each copolymer:$PC_{71}BM$ blend film (see ESI†), with these scans potentially providing evidence for phase-separation at length-scales greater than can be probed *via* GIWAXS. In Fig. 5, out-of-plane GIWAXS patterns are presented for each copolymer:$PC_{71}BM$ blend thin-film having an identical film composition to that of the best performing OPV devices (1 : 4 copolymer:PC71BM wt%). 2D GIWAXS images are provided in the ESI.† From these measurements it can be seen that X-ray scatter from each blend thin-film is dominated by $PC_{71}BM$, as evidenced by the relatively broad ring at $q = 1.34$ $Å^{-1}$ which indicates an isotropic distribution of small fullerene clusters within each blend film.[28]

We note that complimentary measurements on as-cast pure copolymer thin-films only evidence weak X-ray scatter in the out-of-plane direction (see ESI†) with signals attributed to π–π stacking of adjacent copolymers chains at $q_z = 1.72$ $Å^{-1}$ ($d = 3.65$ Å) for PFDT2BT-8 and $q_z = 1.62$ $Å^{-1}$ ($d = 3.88$ Å) for the remaining three copolymers.

Our GIWAXS measurements suggest that the blends studied here are characterised by a finely mixed distribution of copolymer and $PC_{71}BM$ domains with little long-range order present. This conclusion is supported by AFM scans of each blend thin-film surface that are apparently smooth (RMS roughness values below 0.5 nm). Significantly however, we find that the intensity of the broad ring at $q = 1.34$ $Å^{-1}$ (associated with $PC_{71}BM$ aggregation) is largest in the fluorene copolymer PFDT2BT-8:$PC_{71}BM$ blend and is greater than that of X-ray scatter from PCDT2BT-8:$PC_{71}BM$ and the two fused-thiophene polymer blends PCDTTBT-8:$PC_{71}BM$ and PFDTTBT-8:$PC_{71}BM$. This suggests that the degree of $PC_{71}BM$ crystallisation in the polymer blends is different. However, as the linewidth of the scatter peak at $q = 1.34$ $Å^{-1}$ is similar in all blends, we conclude that the average size of the $PC_{71}BM$ aggregates is constant, although the fraction of molecules that find themselves within such an aggregate is different. We propose that enhanced $PC_{71}BM$ aggregation in PFDT2BT-8:$PC_{71}BM$ facilitates the extraction of electrons through the creation of percolation pathways within the BHJ, hence suppressing non-geminate recombination.[29] At present, the origin of the enhanced $PC_{71}BM$ aggregation in PFDT2BT-8:$PC_{71}BM$ blends is not understood.

To determine whether any optical or electronic differences exist between each photovoltaic blend in order to rationalise the solar cell characteristics presented earlier, we have performed time-resolved optical spectroscopy to probe distinct stages in the photocurrent generation process. Specifically, the relative yield of free polarons in the copolymers on the μs timescale was probed using transient absorption spectroscopy (TAS). To compliment these studies, organic field-effect transistor (OFET) devices were fabricated to determine the charge-carrier mobility in each copolymer.

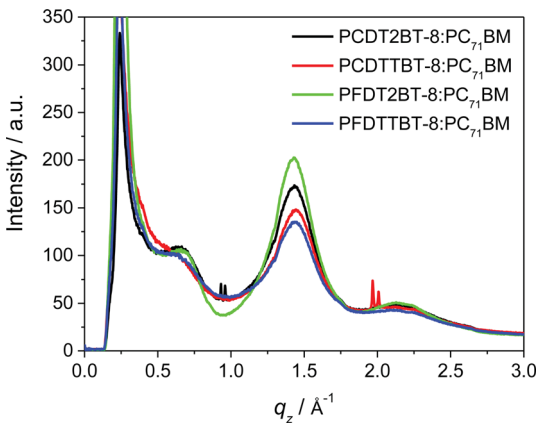

Fig. 5 Out-of-plane GIWAXS profiles of X-ray scatter from 1 : 4 wt% copolymer:$PC_{71}BM$ blend thin-films. Here, the region of zero scattering intensity at low q corresponds to the position of the beam-stop.

To probe the relative yield of charge carriers in the blend, we have performed TAS measurements to monitor the dynamics of hole polarons generated after photoexcitation of the copolymer and subsequent excited state dissociation at a copolymer:$PC_{71}BM$ interface. Note that steady-state photoluminescence (PL) measurements of each copolymer:fullerene blend film indicate efficient (>99%) quenching of photoexcited states (see ESI†). Here, a lower blend concentration of $PC_{71}BM$ (20 wt%) than used in optimised devices was used to slow the recombination of dissociated polarons, as the decay dynamics occurred within a timescale commensurate with the response time of the instrument in blends with compositions corresponding to optimised devices. This data is presented in Fig. 6.

As shown, over the time-range 0.2–2 μs the transient absorption dynamics at 960 nm (corresponding to the peak absorption wavelength by the hole polarons)[30] from each blend thin-film exhibit power-law decays, indicative of non-germinate recombination processes of dissociated polarons.[31,32] As shown, a similar ΔOD is determined for each copolymer:$PC_{71}BM$ blend. Previous studies have shown that the magnitude of ΔOD provides a reasonable indicator of the quantum yield of dissociated charges, with further reports of this signal correlating with photocurrent generation efficiency in a fabricated OPV device.[33] Here however, we do not find sufficient evidence to suggest that variations in polaron yields between each copolymer:$PC_{71}BM$ sample correlate with OPV device efficiency as the different polymers display almost identical charge generation and recombination characteristics. For example, the blend system PFDT2BT-8:$PC_{71}BM$ exhibits the most efficient photovoltaic behaviour, however it displays similar ΔOD transient kinetics to all other blend films studied.

Bottom-gate architecture OFET devices were fabricated to characterise the charge-carrier mobility of each of the copolymers. Transfer and output characteristics for typical copolymer OFETs are presented in the ESI† with extracted charge carrier mobilities detailed in Table 3.

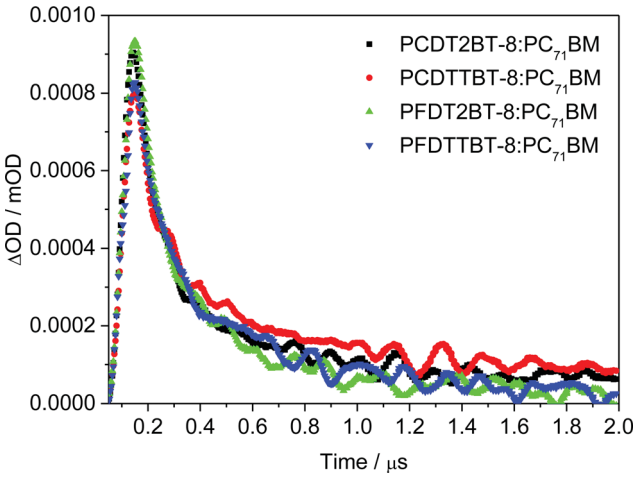

Fig. 6 Transient absorption decays in copolymer:$PC_{71}BM$ (4 : 1 wt%) blend thin-films following excitation at 567 nm. Here, fractional absorption was probed at the hole polaron band located at 960 nm. Spectra are normalised for absorption at the pump wavelength.

Table 3 OFET performance of each polymer. Mobility values in square brackets correspond to the maximum value in each sample set

Polymer	Mobility μ_h[a]/$\times 10^{-3}$ cm^2 V^{-1} s^{-1}	I_{ON}/I_{OFF}[b]	V_T/V
PCDT2BT-8	2.1 ± 0.6 [3.5]	5.5×10^3	−55
PCDTTBT-8	2.3 ± 0.5 [3.1]	3.8×10^3	−54
PFDT2BT-8	4.3 ± 0.7 [5.2]	1.5×10^4	−63
PFDTTBT-8	0.7 ± 0.7 [2.0]	9.8×10^2	−70

[a] Characteristics of devices in the saturation regime. [b] Calculated in the saturation regime.

Here it can be seen that the copolymer PFDT2BT-8 exhibits a higher charge carrier mobility than the thienothiophene derivative PFDTTBT-8 (values of 4.3×10^{-3} cm^2 V^{-1} s^{-1} and 7×10^{-4} cm^2 V^{-1} s^{-1} respectively). A relatively high on/off ratio of 10^4 is also determined for PFDT2BT-8. Furthermore, for the carbazole containing copolymers, mobility values of 2.1×10^{-3} cm^2 V^{-1} s^{-1} and 2.4×10^{-3} cm^2 V^{-1} s^{-1} are obtained for the PCDT2BT-8 and PCDTTBT-8 copolymers respectively. We therefore correlate the best performing solar cell devices that incorporate PFDT2BT-8 with the superior charge carrier mobility of this copolymer compared to the others studied. This characteristic also correlates well with the relatively higher device FF that suggests low charge recombination within the semiconductor blend layer. For the other copolymer blends studied, the relatively lower PCEs of solar cell devices are not found to be limited by the yield of hole polarons. Note that with the exception of PCDT2BT-8:$PC_{71}BM$ devices, all solar cells exhibit comparable photocurrent densities at relatively large reverse bias. This suggests that higher device efficiencies may yet be obtainable in these systems after optimising other properties of the copolymer, for example its molecular weight or purity.[34,35]

Experimental

Materials

PCDT2BT-8,[19] PFDT2BT-8,[18] 9-(heptadecan-9-yl)-2,7-bis-(4,4,5,5-tetramethyl-[1,3,2]dioxaborolan-2-yl)-9*H*-carbazole[9] and 4,7-bis(5-bromothieno[3,2-*b*]thiophen-2-yl)-5,6-bis(octyloxy)-benzo-[*c*][1,2,5]-thiadiazole[36] were prepared according to literature procedures. 9,9-Dioctylfluorene-2,7-diboronic acid bis(1,3-propanediol) ester was obtained commercially. Toluene was dried and distilled over sodium under an inert argon atmosphere. Acetonitrile (high performance liquid chromatography (HPLC) grade) was dried and distilled over phosphorus pentoxide under an inert argon atmosphere, then stored over molecular sieves (3 Å).

Poly[9-(heptadecan-9-yl)-9*H*-carbazole-2,7-diyl-*alt*-(5,6-bis(octyloxy))-4,7-di(thieno[3,2-*b*]thiophen-2-yl)benzo[*c*][1,2,5]thiadiazole-5,5-diyl] PCDTTBT-8

To a degassed solution of 9-(heptadecan-9-yl)-2,7-bis(4,4,5,5-tetramethyl-1,3,2-dioxaborolan-2-yl)-9*H*-carbazole (1.2329 g, 1.875 mmol) and 4,7-bis-(5-bromo-thieno[3,2-*b*]thiophen-2-yl)-5,6-bis-octyloxy-benzo[1,2,5]thiadiazole (1.5502 g, 1.875 mmol)

in toluene (30 cm^3) was added to a degassed solution of tetraethylammonium hydroxide (10 cm^3 of a 20 wt% aqueous solution, 13.54 mmol). $Pd(OAc)_2$ (15.0 mg, 0.0673 mmol) and tri(*o*-tolyl)phosphine (40.8 mg, 0.134 mmol) were subsequently added, followed by degassing the mixture and heating to 95 °C for 72 hours. The mixture was then cooled to room temperature and bromobenzene (0.15 cm^3) was added and the mixture degassed and heated to 90 °C for 1 hour. The mixture was again cooled to room temperature and phenylboronic acid (150 mg) was added and the mixture degassed and heated to 90 °C for 3 hours. After cooling to room temperature, the mixture was dissolved in $CHCl_3$ (300 cm^3) and to this solution was added an ammonium hydroxide solution (28% in H_2O, 200 cm^3). The mixture was heated to reflux over 3 hours and then cooled to room temperature and the organic phase separated. Ethylenediaminetetraacetic acid disodium salt dihydrate (0.500 g, 1.34 mmol) was added to the organic phase and was left to stir overnight. The mixture was then washed with distilled water (2 × 200 cm^3), the organic phase was separated and concentrated to about 50 cm^3 and poured into degassed methanol–water mixture (10 : 1, v/v, 500 cm^3). The resulting mixture was then stirred overnight and the resulting precipitate collected by filtration. This solid was cleaned using Soxhlet extraction with solvents in order methanol, acetone, hexane and toluene. The toluene fraction was concentrated to about 50 cm^3 and then poured into degassed methanol (500 cm^3). The resulting mixture was stirred overnight and the solid collected by filtration to afford the polymer as a red powder (1.75 g, yield 87%). GPC (1,2,4-trichlorobenzene at 100 °C): M_n = 18.600, M_w = 48 000, PD = 2.58. ^1H NMR ($C_2D_2Cl_4$ at 100 °C, δ_H/ppm): 8.74 (s, 2H), 8.07 (s, 2H), 7.77 (s, 2H), 7.61 (s, 2H), 7.55 (br, 2H), 4.69 (br, 1H), 4.18 (s, 4H), 2.39 (br, 2H), 2.07 (br, 2H), 2.00 (br, 4H), 1.51 (br, 4H), 1.49–1.10 (m, 40H), 0.88 (m, 6H), 0.79 (m, 6H). Anal. calcd for $(C_{63}H_{79}N_3O_2S_5)_n$: C, 70.68; H, 7.44; N, 3.92; Br, 0. Found: C, 70.97; H, 7.22; N, 3.77; Br, 0%.

Poly[9,9-dioctyl-9*H*-fluorene-2,7-diyl-*alt*-(5,6-bis(octyloxy))-4,7-di(thieno[3,2-*b*]thiophen-2-yl)benzo[*c*][1,2,5]thiadiazole-5,5-diyl] PFDTTBT-8

To a flask containing 9,9-dioctylfluorene-2,7-diboronic acid bis(1,3-propanediol) ester (0.5403 g, 0.9676 mmol), and 4,7-bis-(5-bromo-thieno[3,2-*b*]thiophen-2-yl)-5,6-bis-octyloxy-benzo-[1,2,5]thiadiazole (0.800 g, 0.9676 mmol) was added toluene (21 cm^3). The solution was degassed then a degassed solution of tetraethylammonium hydroxide (7.0 cm^3, of a 20 wt% aqueous solution, 9.48 mmol) was added. $Pd(OAc)_2$ (8.0 mg, 0.0359 mmol) and tri(*o*-tolyl)phosphine (21.7 mg, 0.0713 mmol) were then added and the mixture was degassed and heated to 95 °C for 48 hours. The mixture was cooled to room temperature and bromobenzene (0.1 cm^3) was added. The mixture was then degassed and heated to 90 °C for 1 hour. The mixture was cooled to room temperature and phenylboronic acid (150 mg) was added. The mixture was then degassed and heated to 90 °C for 3 hours. After cooling to room temperature, the mixture was dissolved in $CHCl_3$ (300 cm^3) and to this solution was added an ammonium hydroxide solution (28% in H_2O, 200 cm^3). The mixture was heated to reflux for 3 hours, cooled to room temperature and the organic phase was separated. Ethylenediaminetetraacetic acid disodium salt dihydrate (0.300 g, 0.80 mmol) was added to the organic phase and was left to stir overnight. The mixture was then washed with distilled water (2 × 200 cm^3), the organic phase was separated and concentrated to about 50 cm^3 and poured into degassed methanol–water mixture (10 : 1, v/v, 500 cm^3). The resulting mixture was then stirred overnight and the resulting precipitate collected by filtration. The collected solid was cleaned using Soxhlet extraction with solvents in order methanol, acetone, hexane and toluene. The toluene fraction was concentrated to about 50 cm^3 and then poured into degassed methanol (500 cm^3). The resulting mixture was stirred overnight and the solid collected by filtration to afford the polymer as a red powder (0.82 g, yield 80%). GPC (1,2,4-trichlorobenzene at 100 °C): M_n = 25.400; M_w = 75 800, PD = 2.98. ^1H NMR ($C_2D_2Cl_4$ at 100 °C, δ_H/ppm): 8.83 (s, 2H), 7.69 (m, 8H), 4.33 (br, 4H), 2.08 (br, 8H), 1.57 (br, 4H), 1.48–1.10 (m, 40H), 0.98 (m, 6H), 0.88 (m, 6H). Anal. calcd for $(C_{63}H_{78}N_2O_2S_5)_n$: C, 71.68; H, 7.45; N, 2.65; Br, 0. Found: C, 71.86; H, 7.25; N, 2.73; Br 0%.

Measurements

Polymer characterisation. Nuclear magnetic resonance (NMR) spectra were recorded on Bruker AMX400 400 MHz NMR spectrometer at 100 °C in $C_2D_2Cl_4$ solutions with TMS as the internal standard. Polymer solutions in 1,2,4-trichlorobenzene at 100 °C were used as samples for GPC analysis. The GPC curves were obtained by the RI-detection method, which was calibrated with a series of polystyrene narrow standards (Polymer Laboratories). Elemental analyses were carried out by the Perkin Elmer 2400 CHN Elemental Analyser for CHN analysis and by the Schöniger oxygen flask combustion method for anion analysis. UV-visible absorption spectra were measured by Hitachi U-2010 Double Beam UV/Visible Spectrophotometer. The absorbance of polymers was measured in solution in chloroform (spectrophotometric grade) at ambient temperature using rectangular quartz cuvettes (light path length = 10 mm) purchased from Sigma-Aldrich. Samples of pristine polymer thin films for UV-visible absorption spectra measurements were prepared by dip coating quartz plates into 1 mg cm^{-3} polymer solutions in chloroform (HPLC grade), with measurements carried out at ambient temperature. Cyclic voltammograms were recorded using a Princeton Applied Research Model 263A Potentiostat/Galvanostat. Measurements were carried out under argon at (25 ± 2) °C. 10 ml of tetrabutylammonium hexafluorophosphate solution in acetonitrile (0.1 mol dm^{-3}) was used as the electrolyte solution. A three electrode system was used consisting of an Ag/Ag^+ reference electrode (silver wire in 0.01 mol dm^{-3} silver nitrate solution in the electrolyte solution), a platinum working electrode (2 mm-diameter smooth platinum disc, area = 3.14×10^{-2} cm^2), and a platinum counter electrode (platinum wire). Polymer thin films were formed by drop casting 1.0 mm^3 of polymer solutions in chloroform (HPLC grade) (1 mg cm^{-3}) onto the working electrode, then

dried in air. Ferrocene was employed as a reference redox system according to IUPAC's recommendation.[37]

OPV device fabrication. Pre-patterned glass-ITO substrates (20 Ω $\square^{-1}$) were purchased from Ossila Limited. The substrates were cleaned by sonication in isopropyl alcohol and deionized water and dried with compressed nitrogen. PEDOT:PSS (HC Stark Clevios P VP AI4083, filtered with 0.45 μm PVDF) was spin cast on top of the cleaned substrates to form a 30 nm thick layer in air which was then annealed at 150 °C prior to transferring to a nitrogen filled glovebox. A subsequent thermal anneal at 150 °C was performed inside the glovebox for 1 h. The active layer (blend of copolymer:$PC_{71}BM$) was dynamically deposited *via* spin casting on the anode buffer layer from a range of solvents. In all cases, the copolymer was dissolved at 4 mg ml^{-1} with a total blend concentration of 12–24 mg ml^{-1} depending on the blend ratio of copolymer to fullerene. The active layer thicknesses were varied by adjusting the spin-coating speed and measured using a surface profiler. The cathode (a bilayer of calcium and aluminium – 5 nm and 100 nm respectively) was thermally evaporated within a vacuum chamber held at a pressure < 10^{-6} mbar. Devices were encapsulated using a UV-treated epoxy (Ossila Limited) before testing. Device performance was tested in air using a Newport 92251A-1000 solar simulator (AM1.5) with NREL certified silicon reference cell at 100 mW $cm.^{-2}$ Here, an aperture mask (0.025 cm^2) was placed over each pixel to accurately define the device area.

GIWAXS. Wide-angle X-ray diffraction patterns were obtained for each copolymer:$PC_{71}BM$ blend thin-film in a grazing-incidence geometry at the I07 beamline at the Diamond Light Source (Didcot, UK). Blend thin-films were deposited onto silicon/native oxide substrates for measurement. Samples were measured within a custom-built cell containing a slight overpressure of helium to minimise background X-ray scatter. For measurement, an 8 keV X-ray beam was incident on the sample surface at a grazing-incidence angle of 0.2°. Data was collected using a Pilatus 2M detector and analysed using the DAWN software package (http://www.dawnsci.org). Silver Behanate powder was used as a calibrant.

Transient absorption spectroscopy. Micro- to milli-second transient absorption spectroscopy was performed on films in a N_2 environment and all data shown is scaled for the fraction of photons absorbed at the excitation wavelength. The samples were excited by a dye laser (Photon Technology International Inc. GL-301) pumped by a nitrogen laser (Photon Technology International Inc. GL-3300) to give a pulse width of 0.6 ns at 4 Hz. Excitation was at 567 nm at an energy of 14 ± 2 μJ cm^{-2}. The samples were probed using a halogen lamp (Bentham, IL1) with a stabilised power supply (Bentham, 605). The probe light was detected using a silicon photodiode and the signal subsequently amplified and passed through electronic band-pass filters to improve the signal to noise ratio. The temporal resolution of the system was around 0.6 μs.

OFET device fabrication & characterisation. Silicon oxide substrates were purchased from Ossila Limited. These were cleaned in sequence by sonication in 1% Hellmanex III solution, hot DI water, isopropyl alcohol, cold DI water and compressed nitrogen. Gold electrodes (50 nm of Au on 1 nm of Cr as adhesion layer) were then thermally evaporated under vacuum onto the silicon oxide to define five transistor channels with width and length equal to 103 μm and 30 μm, respectively. The substrates were then cleaned with oxygen plasma for 30 seconds at $P = 100$ W, treated in a 5 mMol solution of PFBT (pentafluorobenzenethiol, Sigma-Aldrich), dried with compressed nitrogen and transferred to a dry glove box atmosphere. Substrates were then treated with HMDS (hexamethyldisilazane, Sigma-Aldrich) to prepare a hydrophobic surface and to minimise surface trap states prior to deposition of the organic semiconductors. The four copolymer solutions were prepared at a concentration of 2 mg ml^{-1} in chloroform and before use were heated at 45 °C for two hours and filtered with a 0.45 μm PTFE filter. For semiconductor deposition, 25 μl of organic semiconductor solution was spin coated at 1000 rpm for 60 seconds, followed by a drying step at 2000 rpm from 5 seconds. The samples were subsequently left for twenty minutes under mild vacuum to facilitate complete evaporation of casting solvent. No further annealing treatments were applied. Complete OFETs were characterised using a PXI modular source measurement system (National Instruments PXI-4132) integrated with the FACT measurement system developed by Ossila. The gate electrode is provided by the boron-doped silicon wafer (ρ < 0.002 Ω cm), while the silicon oxide acts as gate dielectric with a capacitance per unit area of $C_{Ox} = 1.09 \times 10^{-8}$ F cm^{-2}. The electrical connections with the SMU are provided by thermally evaporated Al/Cr (80/5 nm) contact pads. For each copolymer studied, 15 bottom gate/bottom contact OFETs were fabricated.

Conclusions

In this study two new medium band-gap donor–acceptor copolymers comprising 2,7-carbazole or 2,7-fluorene units positioned between thienothiophene and benzothiadiazole units have been synthesised. A photovoltaic study of copolymer:$PC_{71}BM$ blend thin-films of these two new copolymers as well as those of analogous polymers where the thienothiophene units are replaced with dithienyl units has been conducted with the devices fabricated having power conversion efficiencies ranging between 4 and 6% and open-circuit voltages of approximately 0.9 V. A detailed study employing a range of complimentary techniques probing the structural, optical and electronic properties of the materials have been used to explore the underlying physical differences between the copolymers and provide insight into the device PCEs. We find that thienothiophene substitution is an effective method to modify the optical absorption properties of the copolymers. Optical probes show no discernable differences in the photoexcited state quenching efficiency or charge generation yields between each copolymer:$PC_{71}BM$ blend. Probes of film structure using X-ray scattering reveal that whilst the polymer component is largely amorphous in all cases, the degree of $PC_{71}BM$ crystallinity varies between the different polymer-blends studied. In photovoltaic devices, we find that thienothiophene substitution does not result in improved device efficiency. However we find that improved device efficiency (particularly deriving from improved

fill-factors) is positively correlated with polymer blends in which there is higher hole mobility and more extensive $PC_{71}BM$ crystallisation. These results highlight the complexity in semiconductor design for OPV applications and suggest possible routes for polymer optimisation (for example M_w). For devices incorporating the copolymer PFDT2BT-8, relatively high photovoltaic efficiencies (maximum of 6.2%) have been obtained. This result suggests PFDT2BT-8 holds promise as a suitable semiconductor for single junction organic photovoltaic devices, or as a wide band-gap semiconductor for tandem solar cell devices.

Acknowledgements

We thank EPSRC for funding *via* grants EP/I028641/1 and EP/J017361/1. AJP thanks King Abdulaziz University for financial support *via* grant no. D-004/431. We acknowledge assistance from Tao Wang, Alan Dunbar, Nick Scarratt and Tom Glen and I07 beamline staff at the Diamond Light Source for the GIWAXS measurements.

References

1 G. Li, R. Zhu and Y. Yang, *Nat. Photonics*, 2012, **6**, 153–161.
2 F. C. Krebs, *Sol. Energy Mater. Sol. Cells*, 2009, **93**, 394–412.
3 F. G. Brunetti, R. Kumar and F. Wudl, *J. Mater. Chem.*, 2010, **20**, 2934–2948.
4 S. R. Forrest, *Nature*, 2004, **428**, 911–918.
5 Z. C. He, C. M. Zhong, S. J. Su, M. Xu, H. B. Wu and Y. Cao, *Nat. Photonics*, 2012, **6**, 591–595.
6 E. Bundgaard and F. C. Krebs, *Sol. Energy Mater. Sol. Cells*, 2007, **91**, 954–985.
7 R. S. Kularatne, H. D. Magurudeniya, P. Sista, M. C. Biewer and M. C. Stefan, *J. Polym. Sci., Part A: Polym. Chem.*, 2013, **51**, 743–768.
8 Z. G. Zhang and J. Z. Wang, *J. Mater. Chem.*, 2012, **22**, 4178–4187.
9 N. Blouin, A. Michaud and M. Leclerc, *Adv. Mater.*, 2007, **19**, 2295–2300.
10 Q. Hou, Y. S. Xu, W. Yang, M. Yuan, J. B. Peng and Y. Cao, *J. Mater. Chem.*, 2002, **12**, 2887–2892.
11 D. Muhlbacher, M. Scharber, M. Morana, Z. G. Zhu, D. Waller, R. Gaudiana and C. Brabec, *Adv. Mater.*, 2006, **18**, 2884–2899.
12 Y. Zhang, S. K. Hau, H. L. Yip, Y. Sun, O. Acton and A. K. Y. Jen, *Chem. Mater.*, 2010, **22**, 2696–2698.
13 M. Zhang, Y. Gu, X. Guo, F. Liu, S. Zhang, L. Huo, T. P. Russell and J. Hou, *Adv. Mater.*, 2013, **25**, 4944–4949.
14 A. A. B. Alghamdi, D. C. Watters, H. N. Yi, S. Al-Faifi, M. S. Almeataq, D. Coles, J. Kingsley, D. G. Lidzey and A. Iraqi, *J. Mater. Chem. A*, 2013, **1**, 5165–5171.
15 S. K. Lee, N. S. Cho, S. Cho, S. J. Moon, J. K. Lee and G. C. Bazan, *J. Polym. Sci., Part A: Polym. Chem.*, 2009, **47**, 6873–6882.
16 Q. Fen, X. Y. Hou, Y. Lu, H. Chen, A. M. Liu, X. Hu and N. S. Choon, *Sol. Energy Mater. Sol. Cells*, 2010, **94**, 442–445.
17 A. M. Ballantyne, L. C. Chen, J. Nelson, D. D. C. Bradley, Y. Astuti, A. Maurano, C. G. Shuttle, J. R. Durrant, M. Heeney, W. Duffy and I. McCulloch, *Adv. Mater.*, 2007, **19**, 4544–4547.
18 D. C. Watters, H. Yi, A. J. Pearson, J. Kingsley, A. Iraqi and D. Lidzey, *Macromol. Rapid Commun.*, 2013, **34**, 1157–1162.
19 H. N. Yi, S. Al-Faifi, A. Iraqi, D. C. Watters, J. Kingsley and D. G. Lidzey, *J. Mater. Chem.*, 2011, **21**, 13649–13656.
20 P. L. T. Boudreault, S. Beaupre and M. Leclerc, *Polym. Chem.*, 2010, **1**, 127–136.
21 S. H. Park, A. Roy, S. Beaupre, S. Cho, N. Coates, J. S. Moon, D. Moses, M. Leclerc, K. Lee and A. J. Heeger, *Nat. Photonics*, 2009, **3**, 297–U295.
22 N. Blouin, A. Michaud, D. Gendron, S. Wakim, E. Blair, R. Neagu-Plesu, M. Belletete, G. Durocher, Y. Tao and M. Leclerc, *J. Am. Chem. Soc.*, 2008, **130**, 732–742.
23 S. Beaupre and M. Leclerc, *J. Mater. Chem. A*, 2013, **1**, 11097–11105.
24 E. J. Zhou, S. Yamakawa, Y. Zhang, K. Tajima, C. H. Yang and K. Hashimoto, *J. Mater. Chem.*, 2009, **19**, 7730–7737.
25 Y. Xia, X. Su, Z. He, X. Ren, H. Wu, Y. Cao and D. Fan, *Macromol. Rapid Commun.*, 2010, **31**, 1287–1292.
26 J. C. Bijleveld, R. A. M. Verstrijden, M. M. Wienk and R. A. J. Janssen, *J. Mater. Chem.*, 2011, **21**, 9224–9231.
27 Y. Sun, B. P. Lin, H. Yang and X. H. Gong, *Polymer*, 2012, **53**, 1535–1542.
28 T. Wang, A. J. Pearson, A. D. F. Dunbar, P. A. Staniec, D. C. Watters, H. N. Yi, A. J. Ryan, R. A. L. Jones, A. Iraqi and D. G. Lidzey, *Adv. Funct. Mater.*, 2012, **22**, 1399–1408.
29 F. C. Jamieson, E. B. Domingo, T. McCarthy-Ward, M. Heeney, N. Stingelin and J. R. Durrant, *Chem. Sci.*, 2012, **3**, 485–492.
30 N. Bansal, L. X. Reynolds, A. MacLachlan, T. Lutz, R. S. Ashraf, W. M. Zhang, C. B. Nielsen, I. McCulloch, D. G. Rebois, T. Kirchartz, M. S. Hill, K. C. Molloy, J. Nelson and S. A. Haque, *Sci. Rep.*, 2013, **3**, 1531.
31 T. M. Clarke and J. R. Durrant, *Chem. Rev.*, 2010, **110**, 6736–6767.
32 T. M. Clarke, A. M. Ballantyne, J. Nelson, D. D. C. Bradley and J. R. Durrant, *Adv. Funct. Mater.*, 2008, **18**, 4029–4035.
33 T. M. Clarke, A. Ballantyne, S. Shoaee, Y. W. Soon, W. Duffy, M. Heeney, I. McCulloch, J. Nelson and J. R. Durrant, *Adv. Mater.*, 2010, **22**, 5287–5291.
34 R. S. Ashraf, B. C. Schroeder, H. A. Bronstein, Z. Huang, S. Thomas, R. J. Kline, C. J. Brabec, P. Rannou, T. D. Anthopoulos, J. R. Durrant and I. McCulloch, *Adv. Mater.*, 2013, **25**, 2029–2034.
35 J. J. Intemann, K. Yao, H. L. Yip, Y. X. Xu, Y. X. Li, P. W. Liang, F. Z. Ding, X. S. Li and A. K. Y. Jen, *Chem. Mater.*, 2013, **25**, 3188–3195.
36 X. C. Wang, Y. P. Sun, S. Chen, X. Guo, M. J. Zhang, X. Y. Li, Y. F. Li and H. Q. Wang, *Macromolecules*, 2012, **45**, 1208–1216.
37 G. Gritzner, *Pure Appl. Chem.*, 1990, **62**, 1839–1858.